Building High-level Features
Using Large Scale Unsupervised Learning

Quoc V. Le   QUOCLE@CS.STANFORD.EDU
Marc'Aurelio Ranzato   RANZATO@GOOGLE.COM
Rajat Monga   RAJATMONGA@GOOGLE.COM
Matthieu Devin   MDEVIN@GOOGLE.COM
Kai Chen   KAICHEN@GOOGLE.COM
Greg S. Corrado   GCORRADO@GOOGLE.COM
Jeff Dean   JEFF@GOOGLE.COM
Andrew Y. Ng   ANG@CS.STANFORD.EDU

arXiv:1112.6209v5 [cs.LG] 12 Jul 2012

Abstract

We consider the problem of building high-level, class-specific feature detectors from only unlabeled data. For example, is it possible to learn a face detector using only unlabeled images? To answer this, we train a 9-layered locally connected sparse autoencoder with pooling and local contrast normalization on a large dataset of images (the model has 1 billion connections, the dataset has 10 million 200x200 pixel images downloaded from the Internet). We train this network using model parallelism and asynchronous SGD on a cluster with 1,000 machines (16,000 cores) for three days. Contrary to what appears to be a widely-held intuition, our experimental results reveal that it is possible to train a face detector without having to label images as containing a face or not. Control experiments show that this feature detector is robust not only to translation but also to scaling and out-of-plane rotation. We also find that the same network is sensitive to other high-level concepts such as cat faces and human bodies. Starting with these learned features, we trained our network to obtain 15.8% accuracy in recognizing 22,000 object categories from ImageNet, a leap of 70% relative improvement over the previous state-of-the-art.

1. Introduction

The focus of this work is to build *high-level*, class-specific feature detectors from *unlabeled* images. For instance, we would like to understand if it is possible to build a face detector from only unlabeled images. This approach is inspired by the neuroscientific conjecture that there exist highly class-specific neurons in the human brain, generally and informally known as "grandmother neurons." The extent of class-specificity of neurons in the brain is an area of active investigation, but current experimental evidence suggests the possibility that some neurons in the temporal cortex are highly selective for object categories such as faces or hands (Desimone et al., 1984), and perhaps even specific people (Quiroga et al., 2005).

Contemporary computer vision methodology typically emphasizes the role of *labeled* data to obtain these class-specific feature detectors. For example, to build a face detector, one needs a large collection of images labeled as containing faces, often with a bounding box around the face. The need for large labeled sets poses a significant challenge for problems where labeled data are rare. Although approaches that make use of inexpensive unlabeled data are often preferred, they have not been shown to work well for building high-level features.

This work investigates the feasibility of building high-level features from only *unlabeled* data. A positive answer to this question will give rise to two significant results. Practically, this provides an inexpensive way to develop features from unlabeled data. But perhaps more importantly, it answers an intriguing question as to whether the specificity of the "grandmother neuron" could possibly be learned from unlabeled data. Informally, this would suggest that it is at least in principle possible that a baby learns to group faces into one class

because it has seen many of them and not because it is guided by supervision or rewards.

Unsupervised feature learning and deep learning have emerged as methodologies in machine learning for building features from *unlabeled* data. Using unlabeled data in the wild to learn features is the key idea behind the *self-taught learning* framework (Raina et al., 2007). Successful feature learning algorithms and their applications can be found in recent literature using a variety of approaches such as RBMs (Hinton et al., 2006), autoencoders (Hinton & Salakhutdinov, 2006; Bengio et al., 2007), sparse coding (Lee et al., 2007) and K-means (Coates et al., 2011). So far, most of these algorithms have only succeeded in learning *low-level* features such as "edge" or "blob" detectors. Going beyond such simple features and capturing complex invariances is the topic of this work.

Recent studies observe that it is quite time intensive to train deep learning algorithms to yield state of the art results (Ciresan et al., 2010). We conjecture that the long training time is partially responsible for the lack of high-level features reported in the literature. For instance, researchers typically reduce the sizes of datasets and models in order to train networks in a practical amount of time, and these reductions undermine the learning of high-level features.

We address this problem by scaling up the core components involved in training deep networks: the dataset, the model, and the computational resources. First, we use a large dataset generated by sampling random frames from random YouTube videos.[1] Our input data are 200x200 images, much larger than typical 32x32 images used in deep learning and unsupervised feature learning (Krizhevsky, 2009; Ciresan et al., 2010; Le et al., 2010; Coates et al., 2011). Our model, a deep autoencoder with pooling and local contrast normalization, is scaled to these large images by using a large computer cluster. To support parallelism on this cluster, we use the idea of local receptive fields, e.g., (Raina et al., 2009; Le et al., 2010; 2011b). This idea reduces communication costs between machines and thus allows model parallelism (parameters are distributed across machines). Asynchronous SGD is employed to support data parallelism. The model was trained in a distributed fashion on a cluster with 1,000 machines (16,000 cores) for three days.

Experimental results using classification and visualization confirm that it is indeed possible to build high-level features from unlabeled data. In particular, using a hold-out test set consisting of faces and distractors, we discover a feature that is highly selective for faces.

---

[1] This is different from the work of (Lee et al., 2009) who trained their model on images from one class.

This result is also validated by visualization via numerical optimization. Control experiments show that the learned detector is not only invariant to translation but also to out-of-plane rotation and scaling.

Similar experiments reveal the network also learns the concepts of cat faces and human bodies.

The learned representations are also discriminative. Using the learned features, we obtain significant leaps in object recognition with ImageNet. For instance, on ImageNet with 22,000 categories, we achieved 15.8% accuracy, a relative improvement of 70% over the state-of-the-art. Note that, random guess achieves less than 0.005% accuracy for this dataset.

2. Training set construction

Our training dataset is constructed by sampling frames from 10 million YouTube videos. To avoid duplicates, each video contributes only one image to the dataset. Each example is a color image with 200x200 pixels.

A subset of training images is shown in Appendix A. To check the proportion of faces in the dataset, we run an OpenCV face detector on 60x60 randomly-sampled patches from the dataset (http://opencv.willowgarage.com/wiki/). This experiment shows that patches, being detected as faces by the OpenCV face detector, account for less than 3% of the 100,000 sampled patches

3. Algorithm

In this section, we describe the algorithm that we use to learn features from the unlabeled training set.

3.1. Previous work

Our work is inspired by recent successful algorithms in unsupervised feature learning and deep learning (Hinton et al., 2006; Bengio et al., 2007; Ranzato et al., 2007; Lee et al., 2007). It is strongly influenced by the work of (Olshausen & Field, 1996) on sparse coding. According to their study, sparse coding can be trained on unlabeled natural images to yield receptive fields akin to V1 simple cells (Hubel & Wiesel, 1959).

One shortcoming of early approaches such as sparse coding (Olshausen & Field, 1996) is that their architectures are shallow and typically capture low-level concepts (e.g., edge "Gabor" filters) and simple invariances. Addressing this issue is a focus of recent work in deep learning (Hinton et al., 2006; Bengio et al., 2007; Bengio & LeCun, 2007; Lee et al., 2008; 2009) which build hierarchies of feature representations. In particular, Lee et al (2008) show that stacked sparse RBMs can model certain simple functions of the V2 area of the cortex. They also demonstrate that con-

volutional DBNs (Lee et al., 2009), trained on aligned images of faces, can learn a face detector. This result is interesting, but unfortunately requires a certain degree of supervision during dataset construction: their training images (i.e., Caltech 101 images) are aligned, homogeneous and belong to one selected category.
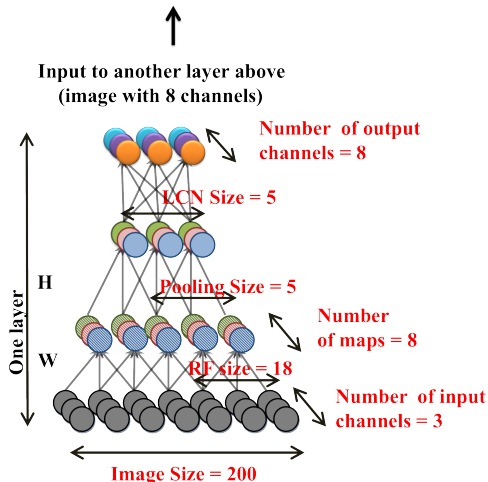

Figure 1. The architecture and parameters in one layer of our network. The overall network replicates this structure three times. For simplicity, the images are in 1D.

3.2. Architecture

Our algorithm is built upon these ideas and can be viewed as a sparse deep autoencoder with three important ingredients: local receptive fields, pooling and local contrast normalization. First, to scale the autoencoder to large images, we use a simple idea known as *local receptive fields* (LeCun et al., 1998; Raina et al., 2009; Lee et al., 2009; Le et al., 2010). This biologically inspired idea proposes that each feature in the autoencoder can connect only to a small region of the lower layer. Next, to achieve invariance to local deformations, we employ local L2 pooling (Hyvärinen et al., 2009; Gregor & LeCun, 2010; Le et al., 2010) and local contrast normalization (Jarrett et al., 2009). L2 pooling, in particular, allows the learning of invariant features (Hyvärinen et al., 2009; Le et al., 2010).

Our deep autoencoder is constructed by replicating three times the same stage composed of local filtering, local pooling and local contrast normalization. The output of one stage is the input to the next one and the overall model can be interpreted as a nine-layered network (see Figure 1).

The first and second sublayers are often known as filtering (or simple) and pooling (or complex) respectively. The third sublayer performs local subtractive and divisive normalization and it is inspired by biological and computational models (Pinto et al., 2008;

Lyu & Simoncelli, 2008; Jarrett et al., 2009).[2]

As mentioned above, central to our approach is the use of local connectivity between neurons. In our experiments, the first sublayer has receptive fields of 18x18 pixels and the second sub-layer pools over 5x5 overlapping neighborhoods of features (i.e., pooling size). The neurons in the first sublayer connect to pixels in all input channels (or maps) whereas the neurons in the second sublayer connect to pixels of only one channel (or map).[3] While the first sublayer outputs linear filter responses, the pooling layer outputs the square root of the sum of the squares of its inputs, and therefore, it is known as L2 pooling.

Our style of stacking a series of uniform modules, switching between selectivity and tolerance layers, is reminiscent of Neocognition and HMAX (Fukushima & Miyake, 1982; LeCun et al., 1998; Riesenhuber & Poggio, 1999). It has also been argued to be an architecture employed by the brain (DiCarlo et al., 2012).

Although we use local receptive fields, they are not convolutional: the parameters are not shared across different locations in the image. This is a stark difference between our approach and previous work (LeCun et al., 1998; Jarrett et al., 2009; Lee et al., 2009). In addition to being more biologically plausible, unshared weights allow the learning of more invariances other than translational invariances (Le et al., 2010).

In terms of scale, our network is perhaps one of the largest known networks to date. It has 1 billion trainable parameters, which is more than an order of magnitude larger than other large networks reported in literature, e.g., (Ciresan et al., 2010; Sermanet & LeCun, 2011) with around 10 million parameters. It is worth noting that our network is still tiny compared to the human visual cortex, which is 10^6 times larger in terms of the number of neurons and synapses (Pakkenberg et al., 2003).

3.3. Learning and Optimization

Learning: During learning, the parameters of the second sublayers (H) are fixed to uniform weights, whereas the encoding weights W_1 and decoding weights W_2 of the first sublayers are adjusted using

---

[2]The subtractive normalization removes the weighted average of neighboring neurons from the current neuron $g_{i,j,k} = h_{i,j,k} - \sum_{iuv} G_{uv} h_{i,j+u,i+v}$ The divisive normalization computes $y_{i,j,k} = g_{i,j,k}/\max\{c, (\sum_{iuv} G_{uv} g_{i,j+u,i+v}^2)^{0.5}\}$, where c is set to be a small number, 0.01, to prevent numerical errors. G is a Gaussian weighting window. (Jarrett et al., 2009)

[3]For more details regarding connectivity patterns and parameter sensitivity, see Appendix B and E.

the following optimization problem

$$\underset{W_1, W_2}{\text{minimize}} \quad \sum_{i=1}^{m} \left(\left\| W_2 W_1^T x^{(i)} - x^{(i)} \right\|_2^2 + \lambda \sum_{j=1}^{k} \sqrt{\epsilon + H_j (W_1^T x^{(i)})^2} \right). \quad (1)$$

Here, λ is a tradeoff parameter between sparsity and reconstruction; m, k are the number of examples and pooling units in a layer respectively; H_j is the vector of weights of the j-th pooling unit. In our experiments, we set $\lambda = 0.1$.

This optimization problem is also known as reconstruction Topographic Independent Component Analysis (Hyvärinen et al., 2009; Le et al., 2011a).[4] The first term in the objective ensures the representations encode important information about the data, i.e., they can reconstruct input data; whereas the second term encourages pooling features to group similar features together to achieve invariances.

Optimization: All parameters in our model were trained jointly with the objective being the sum of the objectives of the three layers.

To train the model, we implemented *model parallelism* by distributing the local weights W1, W2 and H to different machines. A single instance of the model partitions the neurons and weights out across 169 machines (where each machine had 16 CPU cores). A set of machines that collectively make up a single copy of the model is referred to as a "model replica." We have built a software framework called DistBelief that manages all the necessary communication between the different machines within a model replica, so that users of the framework merely need to write the desired upwards and downwards computation functions for the neurons in the model, and don't have to deal with the low-level communication of data across machines.

We further scaled up the training by implementing *asynchronous SGD* using multiple replicas of the core model. For the experiments described here, we divided the training into 5 portions and ran a copy of the model on each of these portions. The models communicate updates through a set of centralized "parameter servers," which keep the current state of all parameters for the model in a set of partitioned servers (we used 256 parameter server partitions for training the model described in this paper). In the simplest implementation, before processing each mini-batch a

model replica asks the centralized parameter servers for an updated copy of its model parameters. It then processes a mini-batch to compute a parameter gradient, and sends the parameter gradients to the appropriate parameter servers, which then apply each gradient to the current value of the model parameter. We can reduce the communication overhead by having each model replica request updated parameters every P steps and by sending updated gradient values to the parameter servers every G steps (where G might not be equal to P). Our DistBelief software framework automatically manages the transfer of parameters and gradients between the model partitions and the parameter servers, freeing implementors of the layer functions from having to deal with these issues.

Asynchronous SGD is more robust to failure and slowness than standard (synchronous) SGD. Specifically, for synchronous SGD, if one of the machines is slow, the entire training process is delayed; whereas for asynchronous SGD, if one machine is slow, only one copy of SGD is delayed while the rest of the optimization can still proceed.

In our training, at every step of SGD, the gradient is computed on a minibatch of 100 examples. We trained the network on a cluster with 1,000 machines for three days. See Appendix B, C, and D for more details regarding our implementation of the optimization.

4. Experiments on Faces

In this section, we describe our analysis of the learned representations in recognizing faces ("the face detector") and present control experiments to understand invariance properties of the face detector. Results for other concepts are presented in the next section.

4.1. Test set

The test set consists of 37,000 images sampled from two datasets: Labeled Faces In the Wild dataset (Huang et al., 2007) and ImageNet dataset (Deng et al., 2009). There are 13,026 faces sampled from *non-aligned* Labeled Faces in The Wild.[5] The rest are distractor objects randomly sampled from ImageNet. These images are resized to fit the visible areas of the top neurons. Some example images are shown in Appendix A.

4.2. Experimental protocols

After training, we used this test set to measure the performance of each neuron in classifying faces against distractors. For each neuron, we found its maximum and minimum activation values, then picked 20 equally

---

[4]In (Bengio et al., 2007; Le et al., 2011a), the encoding weights and the decoding weights are tied: $W_1 = W_2$. However, for better parallelism and better features, our implementation does not enforce tied weights.

[5]http://vis-www.cs.umass.edu/lfw/lfw.tgz

spaced thresholds in between. The reported accuracy is the best classification accuracy among 20 thresholds.

4.3. Recognition

Surprisingly, the best neuron in the network performs very well in recognizing faces, despite the fact that no supervisory signals were given during training. The best neuron in the network achieves 81.7% accuracy in detecting faces. There are 13,026 faces in the test set, so guessing all negative only achieves 64.8%. The best neuron in a one-layered network only achieves 71% accuracy while best linear filter, selected among 100,000 filters sampled randomly from the training set, only achieves 74%.

To understand their contribution, we removed the local contrast normalization sublayers and trained the network again. Results show that the accuracy of best neuron drops to 78.5%. This agrees with previous study showing the importance of local contrast normalization (Jarrett et al., 2009).

We visualize histograms of activation values for face images and random images in Figure 2. It can be seen, even with *exclusively unlabeled data*, the neuron learns to differentiate between faces and random distractors. Specifically, when we give a face as an input image, the neuron tends to output value larger than the threshold, 0. In contrast, if we give a random image as an input image, the neuron tends to output value less than 0.
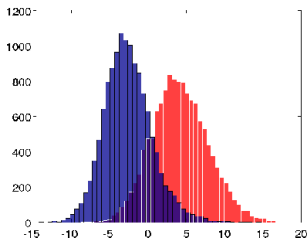
Figure 2. Histograms of faces (red) vs. no faces (blue). The test set is subsampled such that the ratio between faces and no faces is one.

4.4. Visualization

In this section, we will present two visualization techniques to verify if the optimal stimulus of the neuron is indeed a face. The first method is visualizing the most responsive stimuli in the test set. Since the test set is large, this method can reliably detect near optimal stimuli of the tested neuron. The second approach is to perform numerical optimization to find the optimal stimulus (Berkes & Wiskott, 2005; Erhan et al., 2009; Le et al., 2010). In particular, we find the norm-bounded input x which maximizes the output f of the tested neuron, by solving:

$$x^* = \arg\min_x f(x; W, H), \;\; \text{subject to} \;\; ||x||_2 = 1.$$

Here, $f(x; W, H)$ is the output of the tested neuron given learned parameters W, H and input x. In our experiments, this constraint optimization problem is solved by projected gradient descent with line search.

These visualization methods have complementary strengths and weaknesses. For instance, visualizing the most responsive stimuli may suffer from fitting to noise. On the other hand, the numerical optimization approach can be susceptible to local minima. Results, shown in Figure 3, confirm that the tested neuron indeed learns the concept of faces.
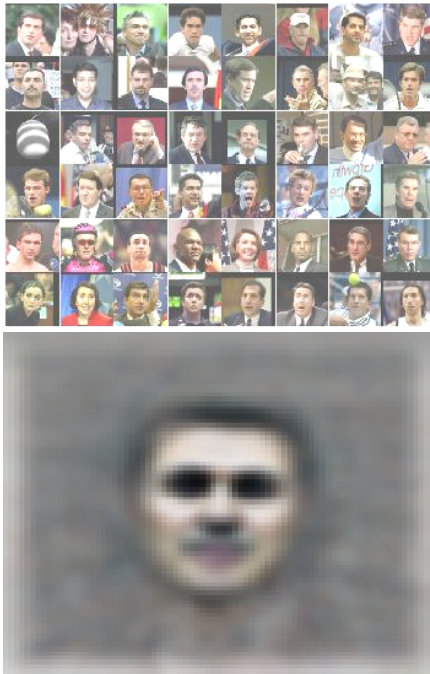
Figure 3. Top: Top 48 stimuli of the best neuron from the test set. Bottom: The optimal stimulus according to numerical constraint optimization.

4.5. Invariance properties

We would like to assess the robustness of the face detector against common object transformations, e.g., translation, scaling and out-of-plane rotation. First, we chose a set of 10 face images and perform distortions to them, e.g., scaling and translating. For out-of-plane rotation, we used 10 images of faces rotating in 3D ("out-of-plane") as the test set. To check the robustness of the neuron, we plot its averaged response over the small test set with respect to changes in scale, 3D rotation (Figure 4), and translation (Figure 5).[6]

_____

[6]Scaled, translated faces are generated by standard cubic interpolation. For 3D rotated faces, we used 10 se-
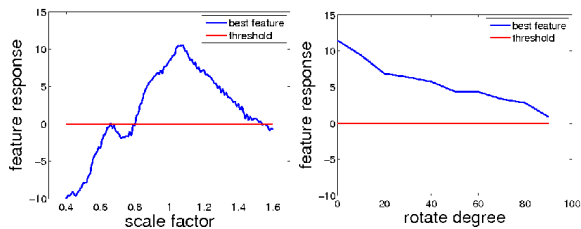
Figure 4. Scale (left) and out-of-plane (3D) rotation (right) invariance properties of the best feature.
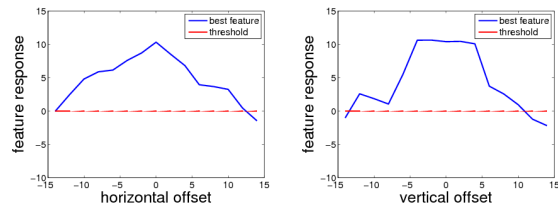

Figure 5. Translational invariance properties of the best feature. x-axis is in pixels

The results show that the neuron is robust against complex and difficult-to-hard-wire invariances such as out-of-plane rotation and scaling.

Control experiments on dataset without faces: As reported above, the best neuron achieves 81.7% accuracy in classifying faces against random distractors. What if we remove all images that have faces from the training set?

We performed the control experiment by running a face detector in OpenCV and removing those training images that contain at least one face. The recognition accuracy of the best neuron dropped to 72.5% which is as low as simple linear filters reported in section 4.3.

5. Cat and human body detectors

Having achieved a face-sensitive neuron, we would like to understand if the network is also able to detect other high-level concepts. For instance, cats and body parts are quite common in YouTube. Did the network also learn these concepts?

To answer this question and quantify selectivity properties of the network with respect to these concepts, we constructed two datasets, one for classifying human bodies against random backgrounds and one for classifying cat faces against other random distractors. For the ease of interpretation, these datasets have a positive-to-negative ratio identical to the face dataset.

The cat face images are collected from the dataset de-

_____

quences of rotated faces from The Sheffield Face Database – http://www.sheffield.ac.uk/eee/research/iel/research/face. See Appendix F for a sample sequence.
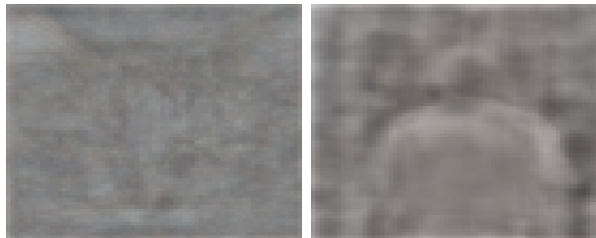

Figure 6. Visualization of the cat face neuron (left) and human body neuron (right).

scribed in (Zhang et al., 2008). In this dataset, there are 10,000 positive images and 18,409 negative images (so that the positive-to-negative ratio is similar to the case of faces). The negative images are chosen randomly from the ImageNet dataset.

Negative and positive examples in our human body dataset are subsampled at random from a benchmark dataset (Keller et al., 2009). In the original dataset, each example is a pair of stereo black-and-white images. But for simplicity, we keep only the left images. In total, like in the case of human faces, we have 13,026 positive and 23,974 negative examples.

We then followed the same experimental protocols as before. The results, shown in Figure 6, confirm that the network learns not only the concept of faces but also the concepts of cat faces and human bodies.

Our high-level detectors also outperform standard baselines in terms of recognition rates, achieving 74.8% and 76.7% on cat and human body respectively. In comparison, best linear filters (sampled from the training set) only achieve 67.2% and 68.1% respectively.

In Table 1, we summarize all previous numerical results comparing the best neurons against other baselines such as linear filters and random guesses. To understand the effects of training, we also measure the performance of best neurons in the same network at random initialization.

We also compare our method against several other algorithms such as deep autoencoders (Hinton & Salakhutdinov, 2006; Bengio et al., 2007) and K-means (Coates et al., 2011). Results of these baselines are reported in the bottom of Table 1.

6. Object recognition with ImageNet

We applied the feature learning method to the task of recognizing objects in the ImageNet dataset (Deng et al., 2009). We started from a network that already learned features from YouTube and ImageNet images using the techniques described in this paper. We then added one-versus-all logistic classifiers on top of the highest layer of this network. This method of initializing a network by unsupervised learning is also

Table 1. Summary of numerical comparisons between our algorithm against other baselines. **Top:** Our algorithm vs. simple baselines. Here, the first three columns are results for methods that do not require training: random guess, random weights (of the network at initialization, without any training) and best linear filters selected from 100,000 examples sampled from the training set. The last three columns are results for methods that have training: the best neuron in the first layer, the best neuron in the highest layer after training, the best neuron in the network when the contrast normalization layers are removed. **Bottom:** Our algorithm vs. autoencoders and K-means.

Concept	Random guess	Same architecture with random weights	Best linear filter	Best first layer neuron	Best neuron	Best neuron without contrast normalization
Faces	64.8%	67.0%	74.0%	71.0%	**81.7%**	78.5%
Human bodies	64.8%	66.5%	68.1%	67.2%	**76.8%**	71.8%
Cats	64.8%	66.0%	67.8%	67.1%	**74.6%**	69.3%

Concept	Our network	Deep autoencoders 3 layers	Deep autoencoders 6 layers	K-means on 40x40 images
Faces	**81.7%**	72.3%	70.9%	72.5%
Human bodies	**76.7%**	71.2%	69.8%	69.3%
Cats	**74.8%**	67.5%	68.3%	68.5%

Table 2. Summary of classification accuracies for our method and other state-of-the-art baselines on ImageNet.

Dataset version	2009 (∼9M images, ∼10K categories)	2011 (∼14M images, ∼22K categories)
State-of-the-art	16.7% (Sanchez & Perronnin, 2011)	9.3% (Weston et al., 2011)
Our method	16.1% (without unsupervised pretraining) **19.2%** (with unsupervised pretraining)	13.6% (without unsupervised pretraining) **15.8%** (with unsupervised pretraining)

known as "unsupervised pretraining." During supervised learning with labeled ImageNet images, the parameters of lower layers and the logistic classifiers were both adjusted. This was done by first adjusting the logistic classifiers and then adjusting the entire network (also known as "fine-tuning"). As a control experiment, we also train a network starting with all random weights (i.e., without unsupervised pretraining: all parameters are initialized randomly and only adjusted by ImageNet labeled data).

We followed the experimental protocols specified by (Deng et al., 2010; Sanchez & Perronnin, 2011), in which, the datasets are randomly split into two halves for training and validation. We report the performance on the validation set and compare against state-of-the-art baselines in Table 2. Note that the splits are not identical to previous work but validation set performances vary slightly across different splits.

The results show that our method, starting from scratch (i.e., raw pixels), bests many state-of-the-art hand-engineered features. On ImageNet with 10K categories, our method yielded a 15% relative improvement over previous best published result. On ImageNet with 22K categories, it achieved a 70% relative improvement over the highest other result of which we are aware (including unpublished results known to the authors of (Weston et al., 2011)). Note, random guess achieves less than 0.005% accuracy for this dataset.

7. Conclusion

In this work, we simulated high-level class-specific neurons using unlabeled data. We achieved this by com-

bining ideas from recently developed algorithms to learn invariances from unlabeled data. Our implementation scales to a cluster with thousands of machines thanks to model parallelism and asynchronous SGD.

Our work shows that it is possible to train neurons to be selective for high-level concepts using entirely unlabeled data. In our experiments, we obtained neurons that function as detectors for faces, human bodies, and cat faces by training on random frames of YouTube videos. These neurons naturally capture complex invariances such as out-of-plane and scale invariances.

The learned representations also work well for discriminative tasks. Starting from these representations, we obtain 15.8% accuracy for object recognition on ImageNet with 20,000 categories, a significant leap of 70% relative improvement over the state-of-the-art.

References

Bengio, Y. and LeCun, Y. Scaling learning algorithms towards AI. In *Large-Scale Kernel Machines*, 2007.

Bengio, Y., Lamblin, P., Popovici, D., and Larochelle, H. Greedy layerwise training of deep networks. In *NIPS*, 2007.

Berkes, P. and Wiskott, L. Slow feature analysis yields a rich repertoire of complex cell properties. *Journal of Vision*, 2005.

Ciresan, D. C., Meier, U., Gambardella, L. M., and

Schmidhuber, J. Deep big simple neural nets excel on handwritten digit recognition. *CoRR*, 2010.

Coates, A., Lee, H., and Ng, A. Y. An analysis of single-layer networks in unsupervised feature learning. In *AISTATS 14*, 2011.

Deng, J., Dong, W., Socher, R., Li, L.-J., Li, K., and Fei-Fei, L. ImageNet: A Large-Scale Hierarchical Image Database. In *CVPR*, 2009.

Deng, J., Berg, A., Li, K., and Fei-Fei, L. What does classifying more than 10,000 image categories tell us? In *ECCV*, 2010.

Desimone, R., Albright, T., Gross, C., and Bruce, C. Stimulus-selective properties of inferior temporal neurons in the macaque. *The Journal of Neuroscience*, 1984.

DiCarlo, J. J., Zoccolan, D., and Rust, N. C. How does the brain solve visual object recognition? *Neuron*, 2012.

Erhan, D., Bengio, Y., Courville, A., and Vincent, P. Visualizing higher-layer features of deep networks. Technical report, University of Montreal, 2009.

Fukushima, K. and Miyake, S. Neocognitron: A new algorithm for pattern recognition tolerant of deformations and shifts in position. *Pattern Recognition*, 1982.

Gregor, K. and LeCun, Y. Emergence of complex-like cells in a temporal product network with local receptive fields. *arXiv:1006.0448*, 2010.

Hinton, G. E. and Salakhutdinov, R.R. Reducing the dimensionality of data with neural networks. *Science*, 2006.

Hinton, G. E., Osindero, S., and Teh, Y. W. A fast learning algorithm for deep belief nets. *Neural Computation*, 2006.

Huang, G. B., Ramesh, M., Berg, T., and Learned-Miller, E. Labeled faces in the wild: A database for studying face recognition in unconstrained environments. Technical Report 07-49, University of Massachusetts, Amherst, October 2007.

Hubel, D. H. and Wiesel, T.N. Receptive fields of single neurons in the the cat's visual cortex. *Journal of Physiology*, 1959.

Hyvärinen, A., Hurri, J., and Hoyer, P. O. *Natural Image Statistics*. Springer, 2009.

Jarrett, K., Kavukcuoglu, K., Ranzato, M.A., and LeCun, Y. What is the best multi-stage architecture for object recognition? In *ICCV*, 2009.

Keller, C., Enzweiler, M., and Gavrila, D. M. A new benchmark for stereo-based pedestrian detection. In *Proc. of the IEEE Intelligent Vehicles Symposium*, 2009.

Krizhevsky, A. Learning multiple layers of features from tiny images. Technical report, University of Toronto, 2009.

Le, Q. V., Ngiam, J., Chen, Z., Chia, D., Koh, P. W., and Ng, A. Y. Tiled convolutional neural networks. In *NIPS*, 2010.

Le, Q. V., Karpenko, A., Ngiam, J., and Ng, A. Y. ICA with Reconstruction Cost for Efficient Overcomplete Feature Learning. In *NIPS*, 2011a.

Le, Q.V., Ngiam, J., Coates, A., Lahiri, A., Prochnow, B., and Ng, A.Y. On optimization methods for deep learning. In *ICML*, 2011b.

LeCun, Y., Bottou, L., Bengio, Y., and Haffner, P. Gradient based learning applied to document recognition. *Proceeding of the IEEE*, 1998.

Lee, H., Battle, A., Raina, R., and Ng, Andrew Y. Efficient sparse coding algorithms. In *NIPS*, 2007.

Lee, H., Ekanadham, C., and Ng, A. Y. Sparse deep belief net model for visual area V2. In *NIPS*, 2008.

Lee, H., Grosse, R., Ranganath, R., and Ng, A.Y. Convolutional deep belief networks for scalable unsupervised learning of hierarchical representations. In *ICML*, 2009.

Lyu, S. and Simoncelli, E. P. Nonlinear image representation using divisive normalization. In *CVPR*, 2008.

Olshausen, B. and Field, D. Emergence of simple-cell receptive field properties by learning a sparse code for natural images. *Nature*, 1996.

Pakkenberg, B., P., D., Marner, L., Bundgaard, M. J., Gundersen, H. J. G., Nyengaard, J. R., and Regeur, L. Aging and the human neocortex. *Experimental Gerontology*, 2003.

Pinto, N., Cox, D. D., and DiCarlo, J. J. Why is real-world visual object recognition hard? *PLoS Computational Biology*, 2008.

Quiroga, R. Q., Reddy, L., Kreiman, G., Koch, C., and Fried, I. Invariant visual representation by single neurons in the human brain. *Nature*, 2005.

Raina, R., Battle, A., Lee, H., Packer, B., and Ng, A.Y. Self-taught learning: Transfer learning from unlabelled data. In *ICML*, 2007.

Raina, R., Madhavan, A., and Ng, A. Y. Large-scale deep unsupervised learning using graphics processors. In *ICML*, 2009.

Ranzato, M., Huang, F. J, Boureau, Y., and LeCun, Y. Unsupervised learning of invariant feature hierarchies with applications to object recognition. In *CVPR*, 2007.

Riesenhuber, M. and Poggio, T. Hierarchical models of object recognition in cortex. *Nature Neuroscience*, 1999.

Sanchez, J. and Perronnin, F. High-dimensional signature compression for large-scale image-classification. In *CVPR*, 2011.

Sermanet, P. and LeCun, Y. Traffic sign recognition with multiscale convolutional neural networks. In *IJCNN*, 2011.

Weston, J., Bengio, S., and Usunier, N. Wsabie: Scaling up to large vocabulary image annotation. In *IJCAI*, 2011.

Zhang, W., Sun, J., and Tang, X. Cat head detection - how to effectively exploit shape and texture features. In *ECCV*, 2008.

A. Training and test images

A subset of training images is shown in Figure 7. As can be seen, the positions, scales, orientations of faces in the dataset are diverse. A subset of test images for
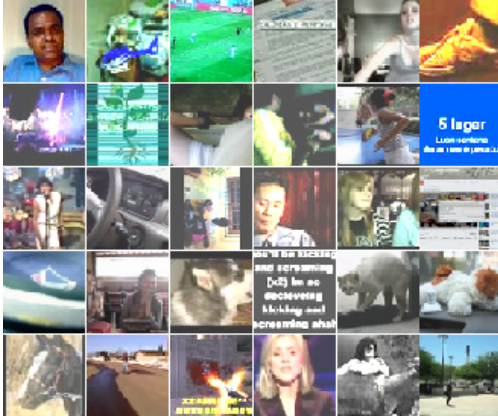

Figure 7. Thirty randomly-selected training images (shown before the whitening step).

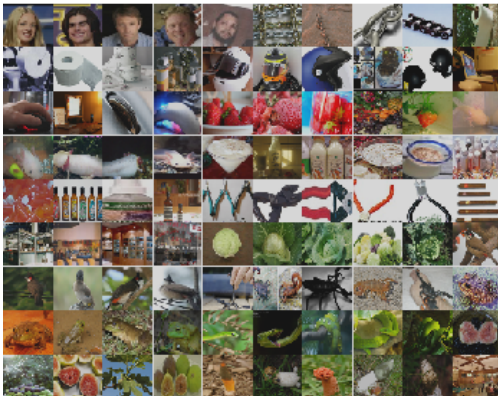identifying the face neuron is shown in Figure 8.

Figure 8. Some example test set images (shown before the whitening step).

B. Models

Central to our approach in this paper is the use of locally-connected networks. In these networks, neurons only connect to a local region of the layer below.

In Figure 9, we show the connectivity patterns of the neural network architecture described in the paper. The actual images in the experiments are 2D, but for simplicity, our images in the visualization are in 1D.
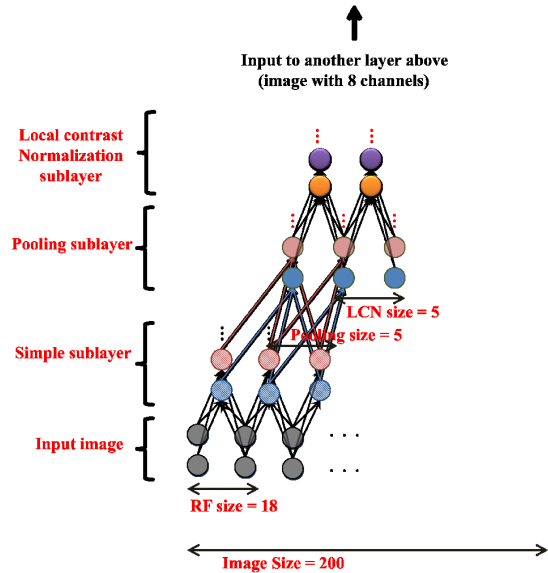
Figure 9. Diagram of the network we used with more detailed connectivity patterns. Color arrows mean that weights only connect to only one map. Dark arrows mean that weights connect to all maps. Pooling neurons only connect to one map whereas simple neurons and LCN neurons connect to all maps.

C. Model Parallelism

We use model parallelism to distribute the storage of parameters and gradient computations to different machines. In Figure 10, we show how the weights are divided and stored in different "partitions," or more simply, machines (see also (Krizhevsky, 2009)).

D. Further multicore parallelism

Machines in our cluster have many cores which allow further parallelism. Hence, we split these cores to perform different tasks. In our implementation, the cores are divided into three groups: reading data, sending (or writing) data, and performing arithmetic computations. At every time instance, these groups work in parallel to load data, compute numerical results and send to network or write data to disks.

E. Parameter sensitivity

The hyper-parameters of the network are chosen to fit computational constraints and optimize the training time of our algorithm. These parameters can be changed at the expense of longer training time or more computational resources. For instance, one could increase the size of the receptive fields at an expense of using more memory, more computation, and more net-
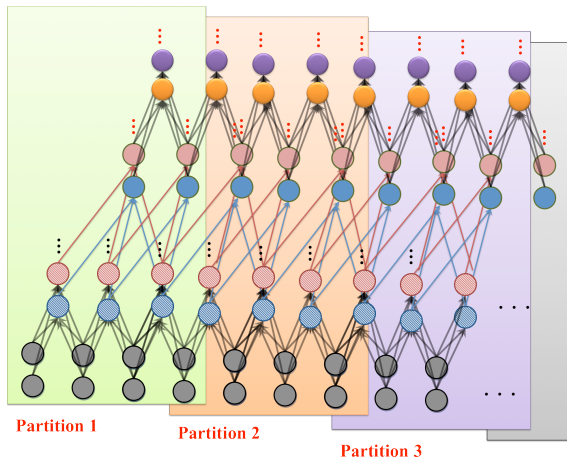
Figure 10. Model parallelism with the network architecture in use. Here, it can be seen that the weights are divided according to the locality of the image and stored on different machines. Concretely, the weights that connect to the left side of the image are stored in machine 1 ("partition 1"). The weights that connect to the central part of the image are stored in machine 2 ("partition 2"). The weights that connect to the right side of the image are stored in machine 3 ("partition 3").

work bandwidth per machine; or one could increase the number of maps at an expense of using more machines and memories.

These hyper-parameters also could affect the performance of the features. We performed control experiments to understand the effects of the two hyper-parameters: the size of the receptive fields and the number of maps. By varying each of these parameters and observing the test set accuracies, we can gain an understanding of how much they affect the performance on the face recognition task. Results, shown in Figure 11, confirm that the results are only slightly sensitive to changes in these control parameters.
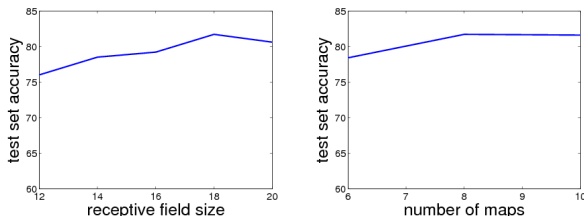

Figure 11. Left: effects of receptive field sizes on the test set accuracy. Right: effects of number of maps on the test set accuracy.

F. Example out-of-plane rotated face sequence

In Figure 12, we show an example sequence of 3D (out-of-plane) rotated faces. Note that the faces are black and white but treated as a color picture in the test. More details are available at the webpage for The Sheffield Face Database dataset – http://www.sheffield.ac.uk/eee/research/iel/research/face

Figure 12. A sequence of 3D (out-of-plane) rotated face of one individual. The dataset consists of 10 sequences.

G. Best linear filters

In the paper, we performed control experiments to compare our features against "best linear filters."

This baseline works as follows. The first step is to sample 100,000 random patches (or filters) from the training set (each patch has the size of a test set image). Then for each patch, we compute its cosine distances between itself and the test set images. The cosine distances are treated as the feature values. Using these feature values, we then search among 20 thresholds to find the best accuracy of a patch in classifying faces against distractors. Each patch gives one accuracy for our test set.

The reported accuracy is the best accuracy among 100,000 patches randomly-selected from the training set.

H. Histograms on the entire test set

Here, we also show the detailed histograms for the neurons on the entire test sets.

The fact that the histograms are distinctive for positive and negative images suggests that the network has learned the concept detectors.
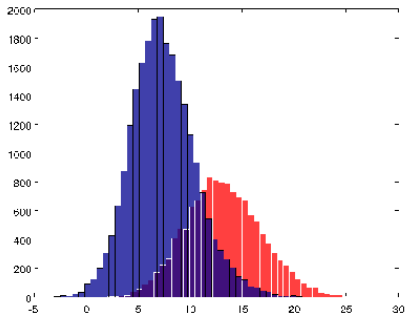
Figure 13. Histograms of neuron's activation values for the best face neuron on the test set. Red: the histogram for face images. Blue: the histogram for random distractors.
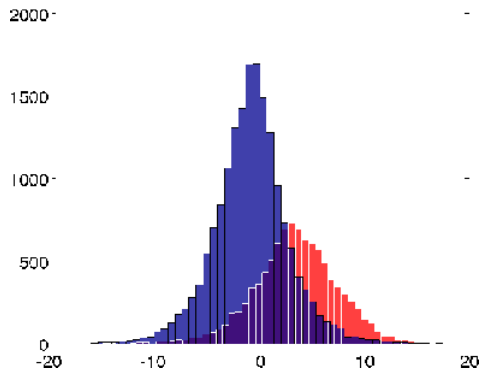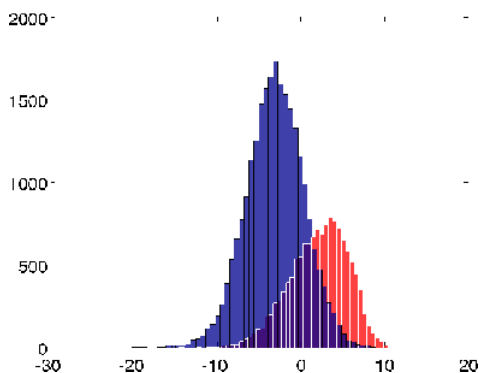

Figure 14. Histograms for the best human body neuron on the test set. Red: the histogram for human body images. Blue: the histogram for random distractors.

I. Most responsive stimuli for cats and human bodies

In Figure 16, we show the most responsive stimuli for cat and human body neurons on the test sets. Note that, the top stimuli for the human body neuron are black and white images because the test set images are black and white (Keller et al., 2009).

J. Implementation details for autoencoders and K-means

In our implementation, deep autoencoders are also locally connected and use sigmoidal activation function. For K-means, we downsample images to 40x40 in order to lower computational costs. We also varied the parameters of autoencoders, K-means and chose them to maximize performances given resource constraints. In our experiments, we used 30,000 centroids for K-means. These models also employed parallelism in a similar fashion described in the paper. They also used 1,000 machines for three days.
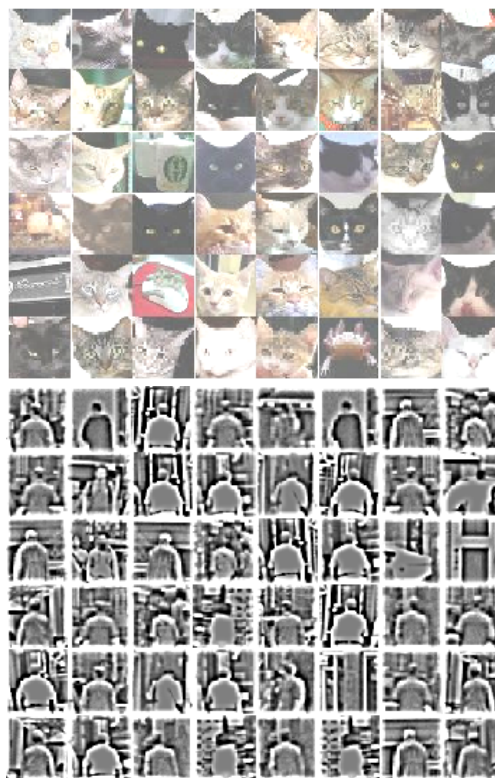

Figure 15. Histograms for the best cat neuron on the test set. Red: the histogram for cat images. Blue: the histogram for random distractors.

Figure 16. Top: most responsive stimuli on the test set for the cat neuron. Bottom: Most responsive human body stimuli on the test set for the human body neuron.